ADVANCES IN ATMOSPHERIC SCIENCES, VOL. 27, NO. 5, 2010, 1064–1077

Modeling Study of Aerosol Indirect Effects on Global Climate with an AGCM

WANG Zhili[1,2] (王志立), ZHANG Hua*[2] (张 华), SHEN Xueshun[3] (沈学顺), Sunling GONG[4,5] (龚山陵), and ZHANG Xiaoye[4] (张小曳)

[1] *Chinese Academy of Meteorological Sciences, Beijing* 100081

[2] *National Climate Center, China Meteorological Administration, Beijing* 100081

[3] *Center for Numerical Prediction Research and State Key Laboratory of Severe Weather, Chinese Academy of Meteorological Sciences, Beijing* 100081

[4] *Center for Atmosphere Watch and Services, China Meteorological Administration, Chinese Academy of Meteorological Sciences, Beijing* 100081

[5] *Air Quality Research Branch, Meteorological Service of Canada, Toronto, Ontario, Canada*

(Received 13 July 2009; revised 28 December 2009)

ABSTRACT

Aerosol indirect effects (AIEs) on global climate were quantitatively investigated by introducing aerosol–cloud interaction parameterizations for water stratus clouds into an AGCM (BCC_AGCM2.0.1), which was developed by the National Climate Center of the China Meteorological Administration. The study yielded a global annual mean of -1.14 W m^{-2} for the first indirect radiative forcing (IRF), with an obvious seasonal change. In summer, large forcing mainly occurred in mid to high latitudes of the Northern Hemisphere, whereas in winter, large values were found at 60°S. The second indirect effect led to global annual mean changes in net shortwave flux of -1.03 W m^{-2} at the top of the atmosphere (TOA), which was relatively significant in mid-latitude regions of both hemispheres. The total AIE reduced the global annual means of net shortwave flux at the TOA and of surface temperature by 1.93 W m^{-2} and 0.12 K, respectively. Change in surface temperature induced by the total AIE was clearly larger in the Northern Hemisphere (-0.23 K) than in the Southern Hemisphere, where changes were negligible. The interhemispheric asymmetry in surface cooling resulted in significant differences in changes of the interhemispheric annual mean precipitation rate, which could lead to a tendency for the ITCZ to broaden. The total AIE decreased the global annual mean precipitation rate by 0.055 mm d^{-1}.

Key words: aerosol, cloud, radiation, indirect effect

Citation: Wang, Z. L., H. Zhang, X. S. Shen, S. L. Gong, and X. Y. Zhang, 2010: Modeling study of aerosol indirect effects on global climate with an AGCM. *Adv. Atmos. Sci.*, **27**(5), 1064–1077, doi: 10.1007/s00376-010-9120-5.

1. Introduction

Cloud, aerosol, and radiation interactions are among the greatest uncertainties in the study of climate change and climate simulation. Aerosol particles can change cloud microphysical properties by acting as cloud condensation nuclei or ice nuclei and thereby alter the radiation balance of the earth–atmosphere system and the cloud lifetime. These effects are called aerosol indirect effects (AIEs) (Forster et al., 2007). When liquid water content is stable in cloud, an increase in aerosol particles can increase the cloud droplet number and decrease the cloud droplet effective radius, leading to an increase in cloud albedo. This is referred to as the first indirect effect (e.g. Junge, 1975; Coakley et al., 1987; Reid et al., 1999;

*Corresponding author: ZHANG Hua, huazhang@cma.gov.cn

Ramaswamy et al., 2001), the cloud albedo effect (e.g. Lohmann and Feichter, 2005), or the Twomey effect (e.g. Twomey, 1977). On the other hand, reduction of the cloud droplet effective radius caused by an increase in aerosol particles can weaken the precipitation efficiency of the cloud and increase the cloud lifetime or liquid water content. This is referred to as the second indirect effect (e.g. Pincus and Baker, 1994; Lohmann and Feichter, 1997; Rotstayn, 1999; Ramaswamy et al., 2001), the cloud lifetime effect (e.g. Lohmann and Feichter, 2005), or the Albrecht effect (e.g. Albrecht, 1989).

The link between aerosol particles and cloud microphysics has been known for a long time. Previous observational studies have shown that smoke from forest fires can increase the cloud droplet number concentration (CDNC) and decrease the cloud droplet effective radius (Warner and Twomey, 1967; Eagan et al., 1974). Over the past few decades, many studies have sought to clarify AIEs. Recent observational studies have advanced understanding of regional and global aerosol effects on climate, especially with regard to low-level stratiform clouds, which constitute a simple cloud system to study relative to many other cloud types. For example, Nakajima et al. (2001) used Advanced Very High Resolution Radiometer (AVHRR) satellite observations to analyze the relationship between column aerosol number concentration and column cloud droplet concentration over ocean and found a positive correlation between them. Jiang et al. (2002) reported that the decrease in cloud liquid water content in some heavily polluted areas would lead to a corresponding decrease in cloud albedo. Zhao et al. (2005) used an aerosol and cloud spectral-bin model to examine the roles of sea-salt and sulfate aerosols in cloud microphysical processes. Their results showed that increases in both sea-salt and sulfate aerosol concentrations could increase the CDNC. Aerosol may also affect both the number concentration and the size of ice nuclei in mixed-phase cloud (Lohmann et al., 2004). Nevertheless, it is still not known whether aerosol particles significantly affect high cirrus cloud, and further research on this subject is needed.

Because of observational limitations, AGCMs have become useful and important tools in the study of AIEs on global climate (e.g. Ghan et al., 2001; Menon et al., 2002; Kristjansson et al., 2005). Jones et al. (2001) and Ming et al. (2005) investigated the effects of anthropogenic sulfate aerosol on cloud albedo and precipitation efficiency by using the Hadley Centre climate model and the Geophysical Fluid Dynamics Laboratory (GFDL) AGCM respectively, and estimated the global mean radiative impacts from both indirect effects to be approximately -1.9 W m^{-2} and -2.3 W m^{-2}, respectively. Kristjansson et al. (2005) studied the aerosol indirect effects due to sulfate and black carbon by using CCM3/NCAR, and showed the total indirect effects induced a globally-averaged cooling of -1.25 K. The IPCC (2007) summarized the results from different models and found that the first indirect effect of anthropogenic aerosols led to radiative forcing from -0.22 to -1.85 W m^{-2} at the top of the atmosphere (TOA), and the second indirect effect led to radiative flux changes from -0.3 to -1.4 W m^{-2} at the TOA. However, many uncertainties remain in the study of AIEs on climate, and further investigation of these effects is thus worthwhile.

The goal of the current study was to provide a more attentive assessment of AIEs on global climate by using a recent version of an AGCM (BCC_AGCM2.0.1) developed by the National Climate Center (NCC) of the China Meteorological Administration (CMA). Section 2 describes the climate model, the parameterization schemes for aerosol–cloud interaction, and the experimental design. Section 3 discusses the effects of various AIEs on shortwave flux and global climate. Finally, conclusions are drawn in section 4.

2. Model description and experimental design

2.1 *Basic model description*

The model was developed by the NCC of the CMA based on the Community Atmosphere Model Version 3 (CAM3) developed by the National Center for Atmospheric Research (NCAR) in the US. However, the dynamics in the model differs significantly from the Eulerian spectral formulation of the dynamical equations in CAM3, and a reference stratified atmospheric temperature and a reference surface pressure were introduced into the model governing equations to improve calculation of the pressure gradient force and the gradients of surface pressure and temperature (Wu et al., 2008). The major modifications on the model physics include a new convection scheme (Zhang and Mu, 2005), a dry adiabatic adjustment scheme in which potential temperature is conserved (Yan, 1987), a modified scheme to calculate sensible heat and moisture fluxes over open ocean that considers the effect of ocean waves on latent and sensible heat fluxes (Wu et al., 2008), and an empirical equation to compute the snow cover fraction (Wu and Wu, 2004).

The model uses horizontal triangular truncation at wavenumber 42 (T42, approximating $2.8^\circ \times 2.8^\circ$) and a vertical hybrid σ-pressure coordinate similar to CAM3, which includes 26 vertical layers with the top layer at the pressure of 2.9 hPa. The radiation scheme in the model is the same as that in CAM3; both models

divide the whole longwave and shortwave region into 19 spectral bands and use a two-stream δ-Eddington approximation (Briegleb, 1992). The cloud fraction was derived from diagnostic relationships introduced by Slingo (1987), with variations described in Hack et al. (1993), Kiehl et al. (1998), and Rasch and Kristjansson (1998). The parameterization of non-convective cloud processes is described in Rasch and Kristjansson (1998), updated by Zhang et al. (2003). The shallow and upper-level convection uses the parameterization from Hack (1994). The radiation parameterization of liquid water cloud was adopted from the scheme given by Slingo (1989). These schemes are also the same as those in CAM3. The deep convection was parameterized following Zhang and Mu (2005). Monthly mean climatological data from 1971–2000 on a Gaussian grid, obtained from the National Centers for Environmental Prediction (NCEP) reanalysis products, were used as the initial model field, and the geographical distribution of sea surface temperature was prescribed based on the 21-year (1981–2001) climatology (available online from http://www/ccsm.ucar.edu/models/atmcam/docs/description). The mass concentrations of aerosols were calculated through an aerosol assimilation system consisting of the Model of Atmospheric Transport and Chemistry (MATCH) and the assimilation of satellite retrievals of aerosol optical depth (Collins et al., 2001, 2002). We included several major aerosol species (e.g. sulfate, organic carbon, black carbon, dust, and sea salt) in our model and treated all aerosol species as an external mixture. The detailed aerosol properties used in the model have been described by Zhang et al. (2009).

Figure 1 illustrates the seasonal changes of the zonal mean of net shortwave flux at the TOA, shortwave cloud forcing and precipitation rate simulated by BCC_AGCM2.0.1 in the experiment TAIE (see section 2.3 for its description). For comparison, observations from the Earth Radiation Budget Experiment (ERBE) (Harrison et al., 1990), and Climate Prediction Center Merged Analysis of Precipitation (CMAP or XIE-ARKIN) product (Xie and Arkin, 1997) are also presented. As shown in Fig. 1, the modeled changes of net shortwave flux at the TOA, shortwave cloud forcing and precipitation rate with latitude were quite consistent with those from observations. The frequencies of occurrence of low-level clouds in the model layers of 934, 854, and 720 hPa (top pressure) in the experiment TAIE were 50%, 53%, and 40%, respectively, whereas their corresponding values from the International Satellite Cloud Climatology Project (ISCCP) were 16%, 26%, and 58%, respectively. In common with most AGCMs, the BCC_AGCM2.0.1 also overestimated the frequency of occurrence of lower-level clouds. More detailed comparisons can be seen in Wu et al. (2008), which showed the overall improvements of climate simulation by BCC_AGCM2.0.1 in comparison with CAM3, especially in the simulation of the tropical maximum and the subtropical minimum of precipitation, the wind stress, sensible and latent heat flux at the ocean surface, etc.

2.2 *Parameterizations for aerosol–cloud interaction*

A number of empirical and prognostic approaches are available for mathematically describing aerosol–cloud interactions. Empirical approaches usually correlate the CDNC with the aerosol mass concentration or aerosol number concentration instead of physical links between aerosols and clouds. Empirical correlations are still used in most AGCM studies at present because they provide a simple and computationally inexpensive way to study AIEs on climate.

For simplicity, we only discuss aerosol effects on water status cloud and describe the relationship between the aerosol mass concentration and CDNC in the model using the scheme given by Menon et al. (2002):

$$N_{\rm d} = \begin{cases} 10^{2.41+0.50\log(C_{\rm s})+0.13\log(C_{\rm c})}, \\ \qquad\qquad\qquad\qquad \text{over land} \\ 10^{2.41+0.50\log(C_{\rm s})+0.13\log(C_{\rm c})+0.051\log C_{\rm ss}}, \\ \qquad\qquad\qquad\qquad \text{over ocean}, \end{cases} \tag{1}$$

where $N_{\rm d}$ is the CDNC (units: $\rm cm^{-3}$); and $C_{\rm s}$, $C_{\rm c}$ and $C_{\rm ss}$ represent the sulfate, organic carbon and sea-salt mass concentration, respectively (units: μg $\rm m^{-3}$). The advantage of the parameterization as given in Eq. (1) is that it implicitly takes into account the physics (updraft velocity, size spectra, growth rate, supersaturation profiles, etc.) that actually determines $N_{\rm d}$. As written in Menon et al. (2002), turbulence has an important role in modifying $N_{\rm d}$ for a given aerosol concentration, so we used the same method and took the cloud top entrainment (CTE) as an indicator of within-cloud turbulence, and scaled $N_{\rm d}$ by a factor that ranged from 1.5 in high CTE (unstable, strong turbulence) conditions to 0.5 in zero CTE (extremely stable, weak turbulence) conditions.

The following formula, proposed by Martin et al. (1994), was adopted for the relationship between the cloud droplet effective radius and CDNC:

$$R_{\rm e} = k\left(\frac{3\rho l}{4\pi\rho_{\rm w}N_{\rm d}}\right)^{\frac{1}{3}}, \tag{2}$$

where R_e is the cloud droplet effective radius (units:

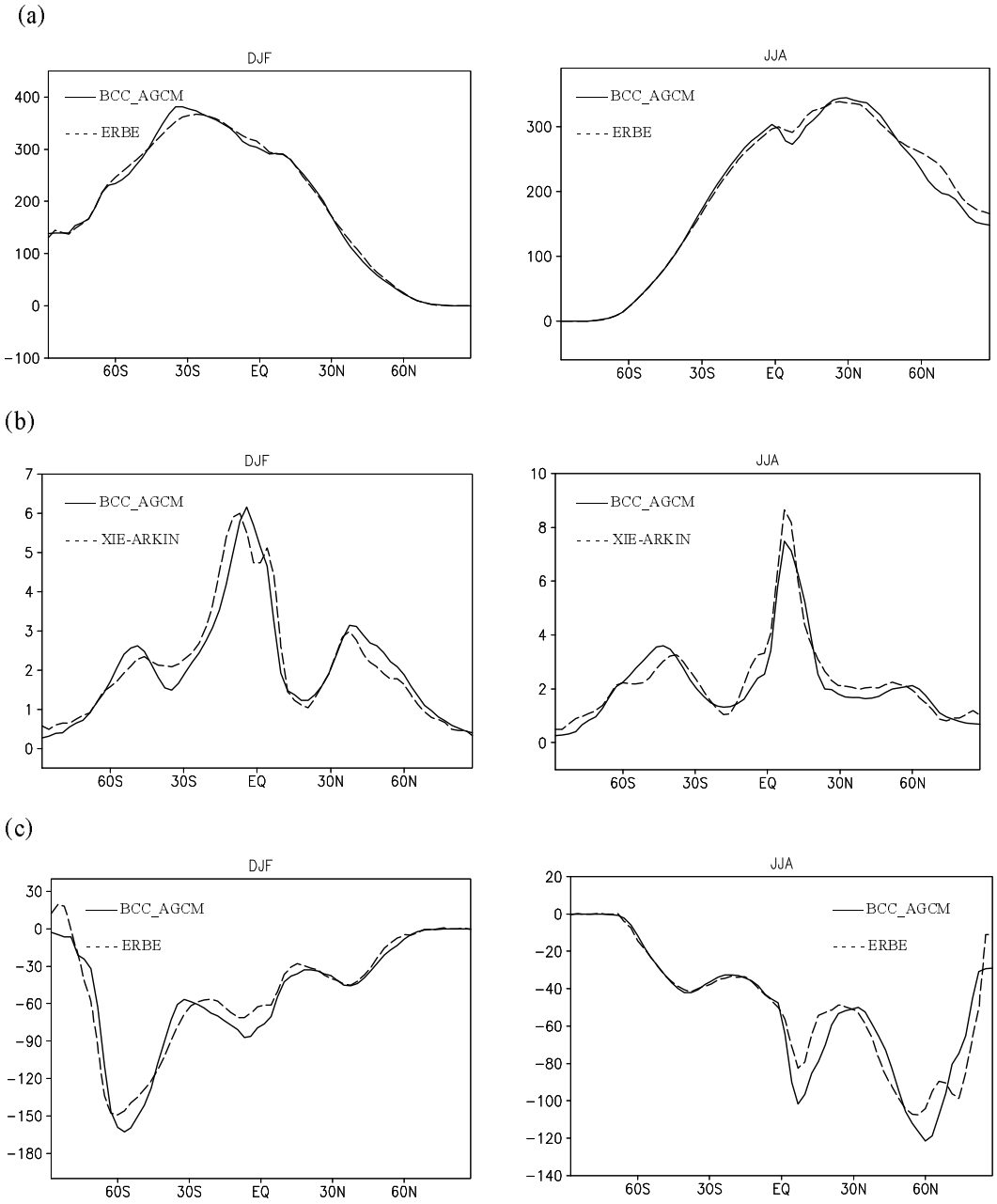

Fig. 1. Zonal mean of (a) net shortwave flux at the TOA (units: W m^{-2}), (b) precipitation rate (units: mm d^{-1}), and (c) shortwave cloud forcing (units: W m^{-2}). DJF and JJA represent winter and summer, respectively.

μm); k is a constant with a value of 1.1; ρ is the air density (units: kg m^{-3}); ρ_w is the water density (units: kg m^{-3}); and l is the cloud liquid water mixing ratio (units: kg kg^{-1}).

The autoconversion rate of cloud water to rain was only determined by the cloud liquid water content in the process of calculating the first indirect effect, using the formula of Sundqvist (1978):

$$P = 10^{-4} l[1 - e^{-(l/l_c)^2}] \,. \tag{3}$$

To evaluate the second indirect effect, we then adopted the autoconversion rate scheme given by Khairoutdinov and Kogan (2000):

$$P = 1350 \times l^{2.47} N_d^{-1.79} \,. \tag{4}$$

In Eqs. (3) and (4), P is the autoconversion rate of cloud water to rain (units: kg kg^{-1} s^{-1}); l_c is a constant equal to 3.0×10^{-4}. Changes in the cloud droplet effective radius and cloud liquid water content can change the cloud optical depth and thus affect

Table 1. Design of the experiments.

Experiments	Description
CONT	Control experiment without aerosol indirect effects and with the parameterization of Sundqvist (1978)
FAIE	First indirect effect with the parameterizations of Menon et al. (2002), Martin et al. (1994), and Sundqvist (1978)
SAIE	Second indirect effect with the parameterization of Khairoutdinov and Kogan (2000)
TAIE	Total aerosol indirect effect with the parameterizations of Menon et al. (2002) Martin et al. (1994), and Khairoutdinov and Kogan (2000)

the cloud radiation process in the model, which can be expressed mathematically by the following formula (Slingo, 1989):

$$\tau = \mathrm{LWP}\left(a + \frac{b}{R_\mathrm{e}}\right) , \tag{5}$$

where τ is the cloud optical depth; LWP is the cloud liquid water path which equals the column liquid water amount per unit area; and a and b are coefficient factors and a function of wavelength referenced from Slingo (1989).

2.3 *Experimental design*

To evaluate various AIEs on climate, four experiments were conducted (Table 1). Experiment CONT was a control test that did not consider any AIEs. To study the first indirect effect, experiment FAIE only included the effect of aerosol on the cloud droplet effective radius. To study the second indirect effect, experiment SAIE only included the effect of aerosol on the precipitation efficiency. Finally, experiment TAIE included both of the above effects to study the total AIE.

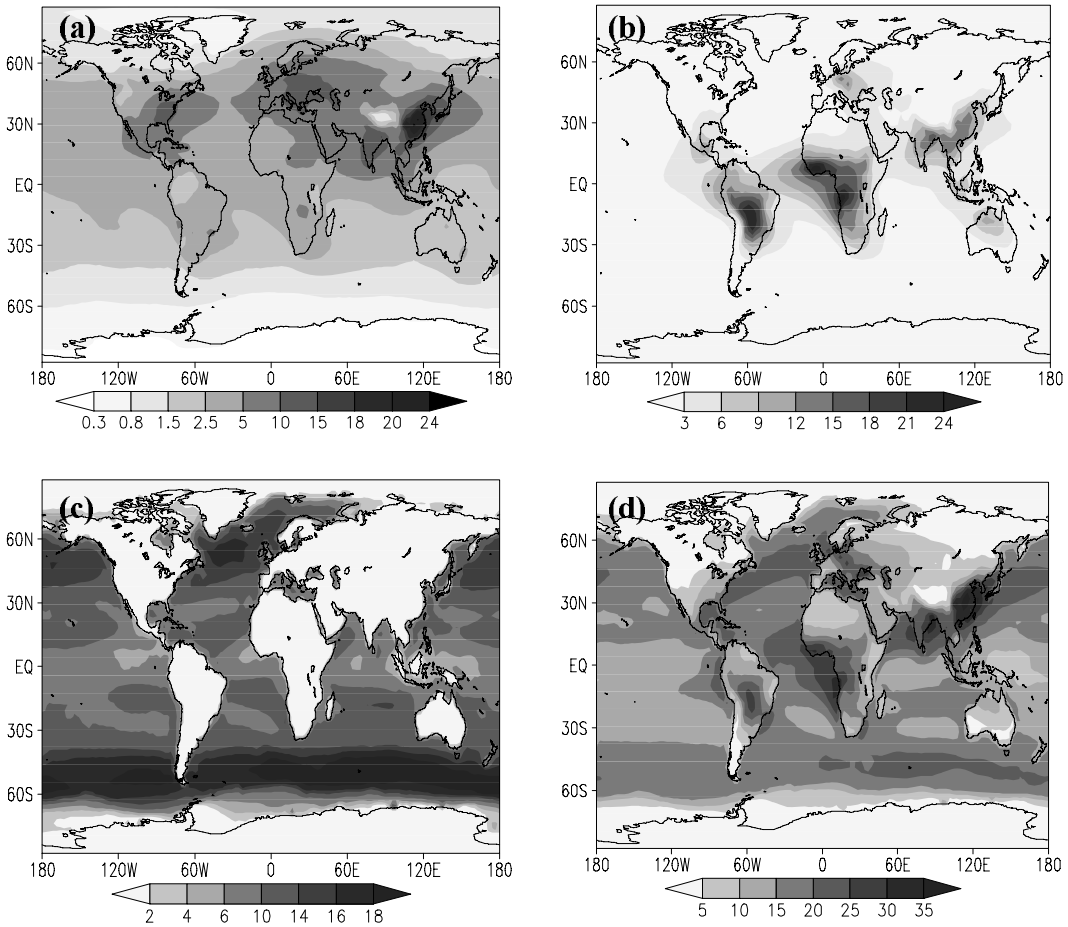

Fig. 2. Global distribution of the annual mean column burden of (a) sulfate, (b) OC, (c) sea-salt, and (d) total aerosol (sulfate+OC+sea-salt) (units: mg m^{-2}).

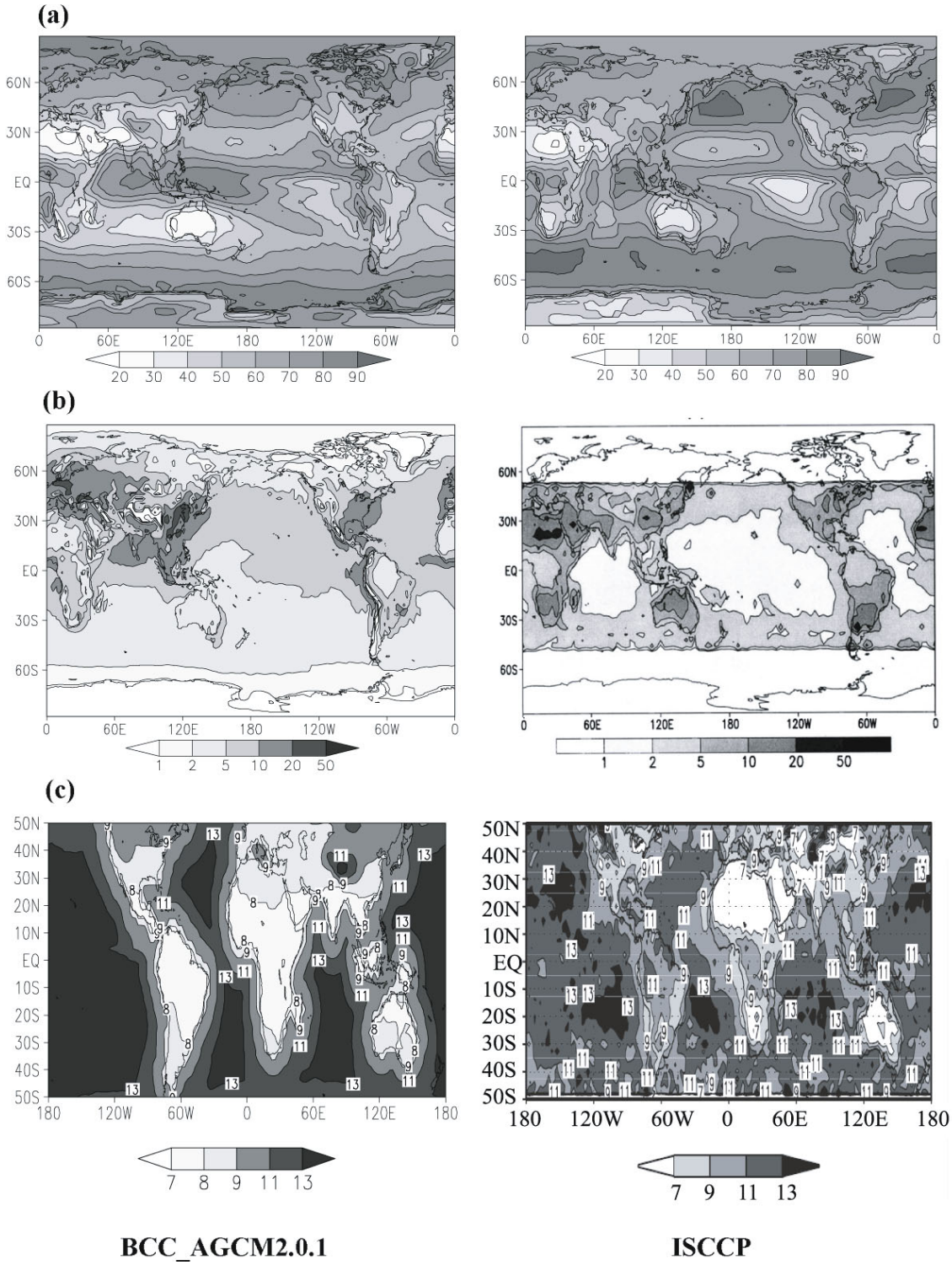

Fig. 3. Global distribution of the annual mean (a) total cloud cover (%), (b) column CDNC (units: 106 cm-2) and (c) cloud droplet effective radius (units: μm). The figures of ISCCP observations in (b) and (c) are from Lohmann et al. (1999) and Kristjansson (2002).

In each experiment, we ran the BCC_AGCM2.0.1 for 11 years, with the first year as the spin-up time. The results for the last 10 years were averaged and analyzed for this study.

3. Results

3.1 *Distribution of the aerosols column burden*

The main precursors of sulfate aerosol are SO_2 produced by anthropogenic sources, volcanic eruptions, and biological sources, especially dimethylsulphide (DMS) oxidation of marine plankton. Organic carbon (OC) aerosol mainly comes from biomass or fossil fuel burning. Sea-salt aerosol is produced by breaking bubbles of seawater at the ocean surface. Figure 2 shows the global distribution of the annual mean column burden of sulfate, OC and sea-salt aerosol used in this study. As shown in Fig. 2, the maximum values of sulfate aerosol column burden were mainly located in East Asia, especially southern, eastern, and northern China, as well as in parts of southeastern North America, Western Europe, and India. Large industrial SO_2 emissions in these land areas lead to maximum sulfate aerosol column burdens of more than 10 mg m^{-2}. Over ocean, sulfate aerosol shows a wide distribution range due to long-distance transport of terrestrial aerosol and marine DMS oxidation. The highest column burdens of OC occurred off the west coast of Central Africa and in the central region of South America, with a maximum value in these regions of approximately 24 mg m^{-2}. There were also OC distributions with local maximum values of around 10 mg m^{-2} over East Asia, India, Western Europe, and northern Australia. The large column burdens of sea-salt aerosol were mainly present over the oceans between 30° and 60° in both hemispheres. Collins et al. (2001, 2002) provided detailed comparisons of modeled aerosol concentrations with observations, and indicated modeled aerosol concentrations were in reasonable agreement with observational values.

3.2 *Global distribution of the column CDNC and cloud droplet effective radius*

Both the CDNC and cloud droplet effective radius are important for estimating AIEs. Figure 3 presents global distributions of simulated total cloud cover and column CDNC and cloud droplet effective radius for low-level clouds from experiment TAIE, and their comparisons with those from ISCCP observations. The simulation of cloud cover was higher than observations at high latitudes, but lower at mid latitudes, which brought about some errors in the simulations of AIEs. The CDNC distribution corresponded well with that of the aerosol concentration, i.e. an increase in the aerosol concentration increased the cloud droplet number but reduced the cloud droplet effective radius. The column CDNC values over land were significantly higher than those over ocean. In contrast, the cloud droplet effective radii greater than 11 μm found over ocean were much larger than the usual values of less than 9 μm found over land. The distributions of simulated column CDNC and cloud droplet effective radius were in reasonable agreement with satellite observations except over the major deserts (Sahara, Gobi, and Australia), because the satellite analysis over the deserts is probably detecting dust rather than cloud droplets (Han et al., 1998). The simulated annual means of R_e averaged between 50°S and 50°N in this work and the satellite retrievals from Han et al. (1994) and Kawamoto et al. (2001) are 11.0, 11.4, and 10.94 μm, respectively. The simulated value was consistent with those of satellite observations.

3.3 *The first IRF*

By the first indirect effect, an increase in aerosol particles in cloud can decrease the cloud droplet effective radius and thus enhance cloud albedo, leading

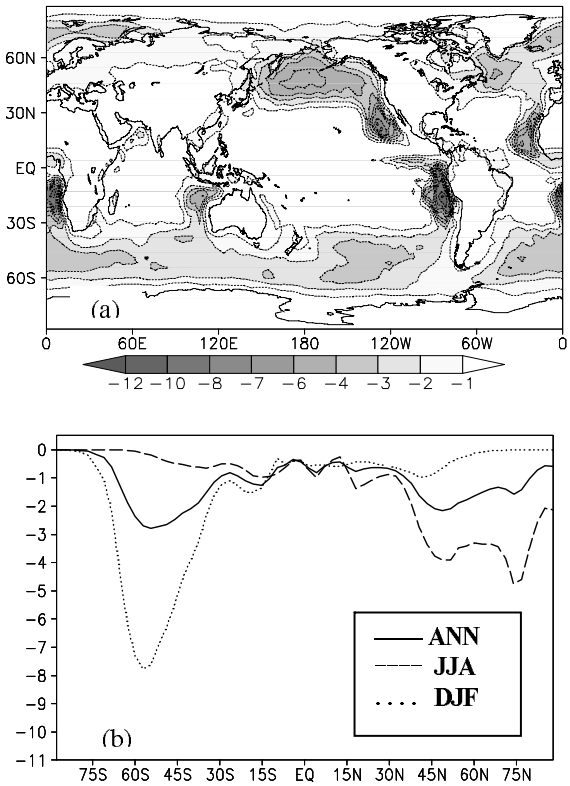

Fig. 4. (a) Global distribution of the annual mean of the first IRF and (b) annual and seasonal zonal means of the first IRF at the TOA. ANN, JJA, and DJF represent the annual, summer, and winter mean values, respectively. (units: W m^{-2})

to negative radiative forcing at the TOA. Figure 4a shows the global distribution of the annual mean of the first IRF at the TOA from experiment FAIE. The simulated results show significantly higher absolute values of the first IRF over ocean than over land, with the opposite pattern found for the aerosol concentration. The four negative radiative forcing centers were located over the North Pacific Ocean, North Atlantic Ocean, and west coasts of the Americas and Africa, with minimum values of -12 W m^{-2}. This result can be explained as follows. Long-range transport of aerosols significantly increases cloud droplet numbers over oceans near aerosol sources; stratus easily forms over these oceans and is readily affected by the aerosols. Jones et al. (2001) and Ming et al. (2005) also obtained similar conclusions. There was a negative center of the first IRF over the northwest coasts of Africa, although the aerosol mass concentration was not high. The likely reason is that the stratus cloud cover is relative abundant over this area and easily affected by the aerosols. In addition, the first IRF over the east coasts of China with very high aerosol abundance was minor because of the underestimation of the stratus cloud cover by BCC_AGCM2.0.1. Furthermore, a zone between 30°S and 60°S over ocean clearly exhibited negative forcing values less than -2 W m^{-2}. In contrast, absolute values of negative forcing over land were relatively low (most less than 1 W m^{-2}). Here, the global annual mean of the first IRF was estimated to be -1.14 W m^{-2}.

Figure 4b shows the zonal mean change of the first IRF at the TOA with latitude from experiment FAIE. The annual mean of the first IRF appears to have a bimodal distribution, with peaks located at approximately 50°S and 50°N. In summer, large absolute values of negative forcing mainly occurred in the mid to high latitudes of the Northern Hemisphere due to anthropogenic aerosol emissions. However, in winter, maximum absolute values of negative forcing were found at approximately 60°S over ocean, where a minimum of -8 W m^{-2} created by the sea-salt aerosol, the oxidation of marine DMS into sulfate aerosol, large amounts of cloud cover, and abundant cloud water content, allowed for more significant interaction between aerosol particles and clouds. This result suggests that the effect of natural aerosol sources on global climate by AIEs cannot be neglected.

3.4 *Shortwave flux changes due to the second indirect effect*

The second indirect effect can weaken the precipitation efficiency and increase the cloud lifetime or cloud condensation water, thus altering the cloud–radiation process and all-sky radiative flux. Therefore, the radiative flux changes at the TOA were used to evaluate the second indirect effect. Figure 5a presents the distribution of net shortwave flux changes due to the second indirect effect at the TOA from the difference between experiment SAIE and CONT. As shown in the figure, although the net shortwave flux changes could be positive or negative, most were negative, with centers over the northern Indian Ocean, western Pacific Ocean, and the regions between 30° and 60° of both Hemispheres. There were two positive centers over the eastern Pacific Ocean and eastern Atlantic Ocean because of the obvious decreasing in total cloud cover after climate response to the second indirect effect. The global annual mean of these changes was -1.03 W m^{-2}.

Figure 5b shows the annual and seasonal zonal means of net shortwave flux change at the TOA from the difference between experiment SAIE and CONT.

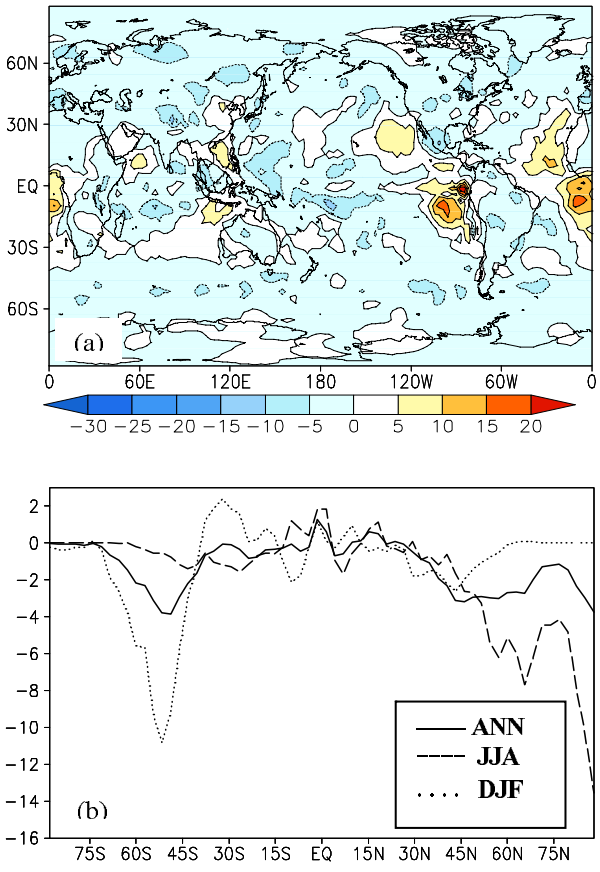

Fig. 5. (a) Global distribution of annual mean net shortwave flux change and (b) the annual and seasonal zonal means of net shortwave flux change at the TOA due to the second indirect effect. ANN, JJA, and DJF represent the annual, summer, and winter mean values, respectively. (units: W m^{-2})

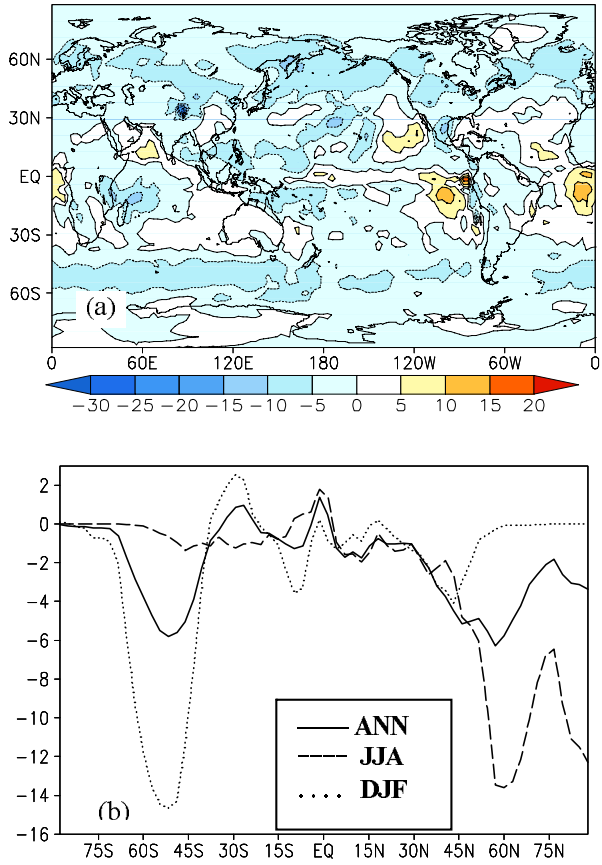

Fig. 6. As in Fig. 5 but for the total AIE. ANN, JJA, and DJF represent the annual, summer, and winter mean values, respectively.

The annual mean demonstrates that the second indirect effect was relatively significant in mid-latitude regions of the Southern Hemisphere, and in mid to high latitude regions of the Northern Hemisphere, with a maximum change of -4.0 W m^{-2} or so. In summer, large absolute values of shortwave flux change mainly occurred in the mid to high latitudes of the Northern Hemisphere. However, in winter, maximum absolute values of shortwave flux change were found at about 50°S over ocean, with a minimum of -11.0 W m^{-2}.

3.5 *Climate response to AIEs*

AIEs can affect the climatic system, mainly by changing cloud radiation. Figure 6 presents the distribution of net shortwave flux changes and the annual and seasonal zonal means of net shortwave flux change at the TOA due to the total AIE from the difference between experiment TAIE and CONT. As shown in Fig. 6a, the distribution of net shortwave flux changes due to the total AIE was similar to that due to the second indirect effect, but the negative changes were obviously enhanced in the regions between 30° and 60° in both hemispheres, and the positive changes were weakened over the eastern Pacific Ocean and eastern Atlantic Ocean. From Fig. 6b, it can be seen that the change trends of annual and seasonal zonal means due to the total AIE were also similar to those due to the second indirect effect, but the negative changes were enhanced between 45°S and 60°S in winter and between 45°N and 60°N in summer, respectively.

Table 2 summarizes various AIEs on meteorological parameters. Among these, the annual mean net shortwave radiative flux at the TOA changed by approximately -1.61 W m^{-2} due to the first indirect effect. Therefore, the annual mean surface temperature was decreased by 0.075 K due to the reduced radiation at the surface, and the annual mean shortwave cloud forcing was decreased by 1.39 W m^{-2} due to the increase in cloud albedo. The first indirect effect had little impact on longwave radiative flux, precipitation and cloud cover. The second indirect effect decreased the annual mean precipitation rate by 0.056 mm d^{-1} and increased the annual mean total cloud liquid water path by 68.77 g m^{-2}. Note, that the latter value might be slightly large because of overestimation of the

Table 2. Annual mean changes in net shortwave and longwave flux at the TOA (FSNT and FLNT) and net shortwave flux at the surface (FSNS), shortwave and longwave cloud forcing (SWCF and LWCF), total cloud liquid water path (LWP), total cloud fraction (CLDTOT), surface temperature (TS), and precipitation rate (PR) due to AIEs, respectively.

	FAIE-CONT	SAIE-CONT	TAIE-CONT
ΔFSNT (W m^{-2})	−1.61	−1.03	−1.93
ΔFLNT (W m^{-2})	−0.091	−0.01	−0.090
ΔFSNS (W m^{-2}	−1.58	−1.31	−2.14
ΔSWCF (W m^{-2})	−1.39	−0.83	−1.54
ΔLWCF (W m^{-2})	−0.038	−0.15	−0.18
ΔLWP (g m^{-2})	0.50	68.77	69.08
ΔCLDTOT (%)	0.1	−1.60	−1.60
ΔTS (K)	−0.075	−0.064	−0.12
ΔPR (mm d^{-1})	0.0069	−0.056	−0.055

*FAIE-CONT, SAIE-CONT and TAIE-CONT represent the first, second and total.

cloud liquid water path by BCC_AGCM2.0.1. The increase in the cloud water path led to an increase in cloud albedo, resulting in a 0.83 W m^{-2} decrease in the annual mean shortwave cloud forcing. The shortwave radiative fluxes arriving at the surface were then reduced, followed by a corresponding decrease of 0.064 K in the annual mean surface temperature. Like the first indirect effect, the second indirect effect had little impact on longwave radiative flux. However, unlike the first indirect effect, the second indirect effect led to a decrease of 1.6% in total cloud cover since the mid and high cloud covers were decreased due to the climate response to the second indirect effect, which caused a decrease in the total cloud cover (figures not shown). However, the exact mechanism is not yet clear and needs to be studied further in the future.

Here, the total AIE on the climatic fields was approximated as the linear sum of the first and second indirect effects, except the changes of shortwave flux. The change in annual mean net shortwave radiative flux at the TOA by total AIE was -1.93 W m^{-2}, with decreases of approximately 0.12 K in surface temperature and 0.055 mm d^{-1} in the precipitation rate. Surface temperature in the Northern Hemisphere decreased by a larger magnitude than in the Southern Hemisphere (by -0.23 K and -0.009 K, respectively). Temperature decreases were mainly found in mid to high latitudes of the Northern Hemisphere, especially in the Arctic regions, where annual mean temperature dropped by approximately 2 K (Fig. 7). The interhemispheric asymmetry in surface cooling resulted in significant differences in changes of interhemispheric annual mean precipitation rate, and the decrease in precipitation rate in the Northern Hemisphere was almost 1.5 times than that in the Southern Hemisphere. The maximum precipitation rate decreased by a rate

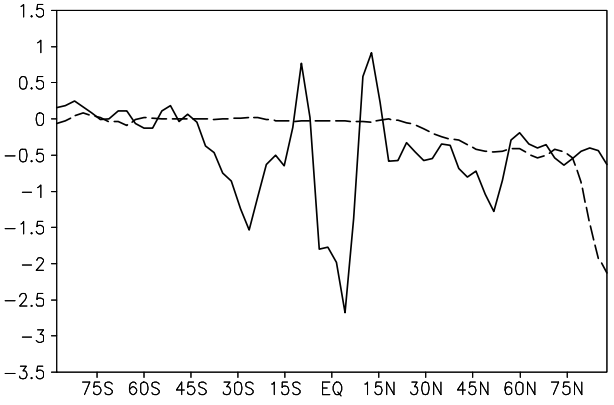

Fig. 7. Annual zonal mean changes in precipitation rate (units: 10^{-1} mm d^{-1}) (solid line) and surface temperature (units: K) (dashed line) due to the total AIE.

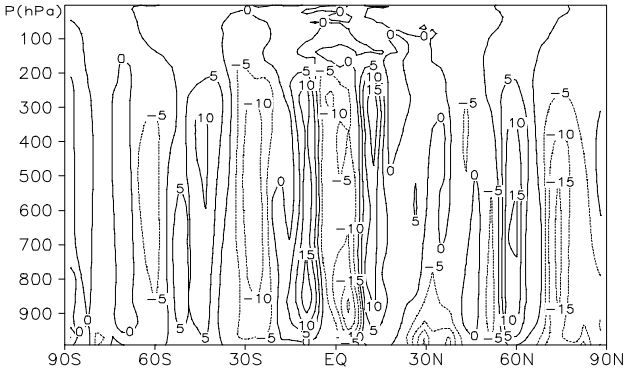

Fig. 8. Latitude–height cross section of zonal mean vertical velocity change due to the total AIE (units: -10^{-2} hPa s^{-1}).

of 0.3 mm d^{-1} north of and near to the equator (close to 5°N). However, the precipitation rate on both the south and north sides of the equator was evidently increased to balance the maximal decrease of water vapor over the equator. Consistently, there were positive vertical velocity changes on both the north and south sides of the equator over which negative vertical velocity change prevailed. The change on the north side was somewhat weaker than that on the south side (Figs. 7 and 8). These changes could lead to a tendency for the ITCZ to broaden.

Figures 9 illustrates the global distributions of annual mean total cloud cover, shortwave cloud forcing, precipitation rate and surface temperature changes caused by the total AIE. Good physical consistency is shown among the distributions and magnitudes of these variables. Increased cloud cover means that more solar radiation will be reflected back to space, creating stronger shortwave cloud forcing and more precipitation, and thus a decrease in surface temperature, especially over land in the Northern Hemisphere, and vice versa. However, there were some inconsistencies over the North Pacific Ocean, and over the oceans at around 60°S, between total cloud cover and shortwave cloud forcing changes due to the underestimation of cloud over in these regions by the model. Figure 9c also clearly shows decreased precipitation over most parts of the equator but increased precipitation on the south and north sides of the equator. Furthermore, it can be seen from Fig. 9c that the total AIE induced a significant decrease in precipitation rate over all land areas in the Asian monsoon regions.

4. Conclusions

Through the introduction of parameterizations proposed by Menon et al. (2002) and Khairoutdinov and Kogan (2000) into BCC_AGCM2.0.1, we simulat-

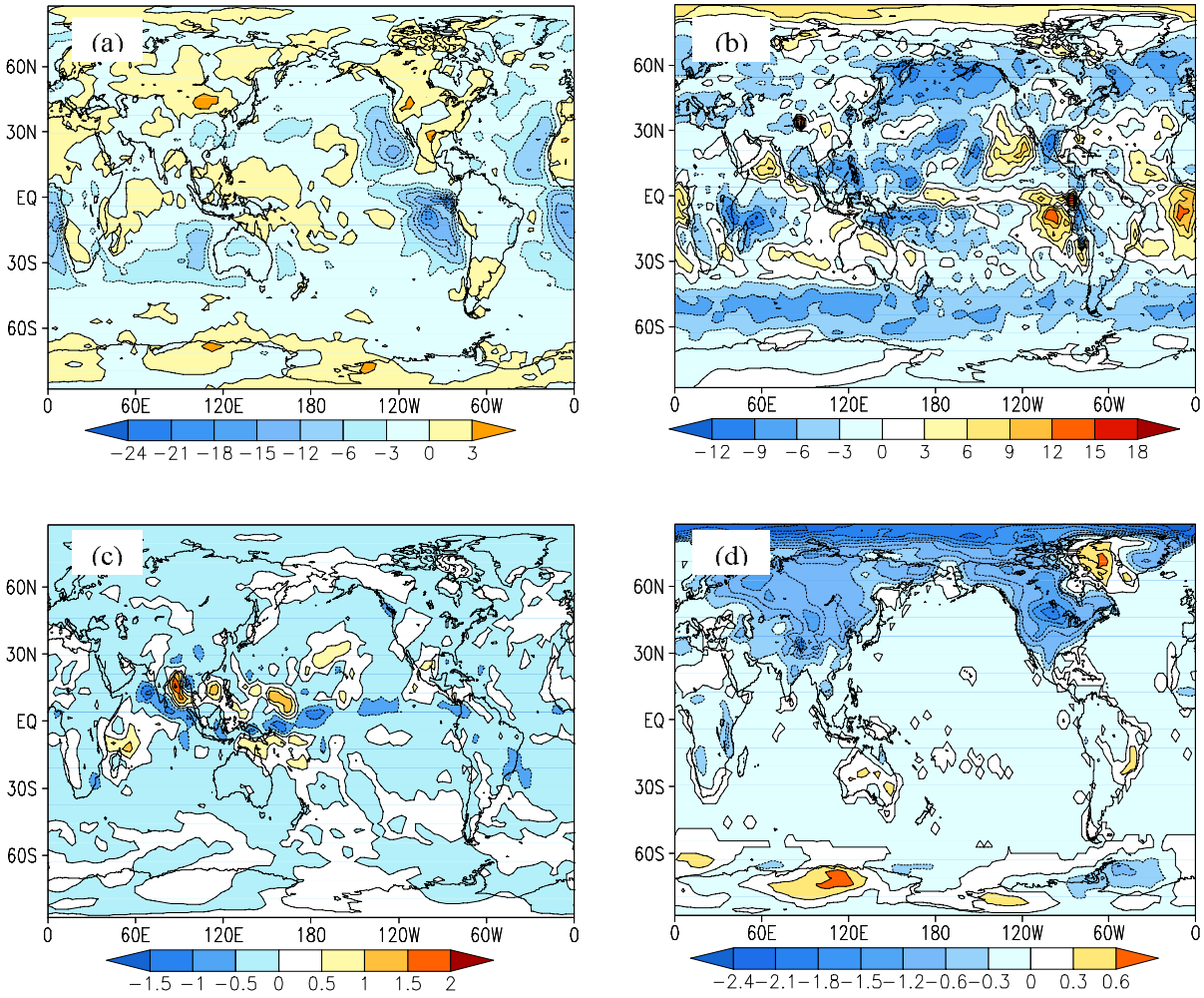

Fig. 9. Global distribution of annual mean changes in (a) total cloud cover (%), (b) shortwave cloud forcing (units: W m^{-2}), (c) precipitation rate (units: mm d^{-1}), and (d) surface temperature (units: K) due to the total AIE.

ed AIEs, including the cloud albedo effect and cloud lifetime effect, on global climate. More species of hygroscopic aerosols were considered in the present study than in the works of Jones et al. (2001) and Ming et al. (2005), which only considered sulfate aerosol, and the work of Kristjansson et al. (2005), which considered sulfate and black carbon. The main findings of this work can be summarized as follows.

First, the global annual mean of the first IRF was −1.14 W m^{-2}; this value was within the range given by the IPCC (2007) (Forster et al., 2007), and the absolute value was less than in Jones et al. (2001) and Ming et al. (2005). The absolute values of the first IRF over ocean were significantly higher than those over land. Of these, the four maximum centers were located over the North Pacific Ocean, North Atlantic Ocean, and west coasts of the Americas and Africa, with a value of approximately −12 W m^{-2}. A clear negative radiative forcing zone was found over ocean between 30°S and 60°S, attributable to sulfate aerosol formation due to the oxidation of marine DMS and sea-salt aerosol. However, the first IRF over the east coasts of China was minor because of the underestimation of the stratus cloud cover by BCC_AGCM2.0.1. The absolute values of negative radiative forcing were lower over land. The first IRF had noticeable seasonal differences: in summer, its maxima were located mainly in the mid and high latitudes of the Northern Hemisphere, whereas in winter, they were located over ocean at approximately 60°S.

Second, changes in net shortwave flux at the TOA due to the second indirect effect were found to be positive or negative; most of these changes, however, were negative. The global annual mean in net shortwave flux changes was −1.03 W m^{-2}, which was larger in magnitude than the results of Jones et al. (2001), Takemura et al. (2005) and Ming et al. (2005), which were −0.5 W m^{-2}, −0.4 W m^{-2}, and −0.9 W m^{-2}, respec-

tively. The second indirect effect was relatively significant in mid-latitude regions of the Southern Hemisphere and in mid to high latitude regions of the Northern Hemisphere, and it also had distinct seasonal differences.

Finally, the two kinds of AIEs were found to be able to enhance cloud albedo and thus reduce radiative flux into the earth–atmosphere system. The total AIE changed annual mean net shortwave flux by -1.93 W m^{-2} at the TOA, changing shortwave cloud forcing by -1.54 W m^{-2} and surface temperature by approximately -0.12 K. Maximum decreases in temperature were found at the mid and high latitudes of the Northern Hemisphere, and the annual mean surface temperature decrease was higher on land than in the ocean, similar to the findings of Takemura et al. (2005). The annual mean precipitation rate change caused by the total AIE was -0.055 mm d^{-1}, with large differences between the Northern and Southern Hemispheres due to interhemispheric asymmetry in surface cooling. The largest reduction in the precipitation rate occurred over the equator; however, the precipitation rate was obviously increased on the south and north sides of the equator, which could lead to broadening of the ITCZ system. Furthermore, the total AIE also produced decreased precipitation rates over all land areas in the Asian monsoon regions.

This study has quantitatively discussed AIEs on global climate. The authors have focused only on water stratus clouds because no reliable parameterization schemes for convective and ice clouds are currently available. The aerosol model described here was coupled offline with the AGCM, rather than online, as in Menon et al. (2002). This may have introduced large errors in the estimations of AIEs, especially in the evaluation of climate response to AIEs. In addition, the absorbing aerosols (such as black carbon and dust) were not considered in the current study of AIEs because absorbing aerosols produce very different AIEs from scattering aerosols (such as sulfate, organic carbon, and sea salt) considered in the current paper. Therefore, a more complete picture of aerosol indirect effects should include absorbing aerosols, and this will be studied in future work.

Acknowledgements. This work was financially supported by the National Basic Research Program of China (Grant No. 2006CB403707), the Public Meteorology Special Foundation of MOST (Grant Nos. GYHY200706036 and 2010CB955608), and the National Key Technology R&D Program (Grant Nos. 2007BAC03A01 and 2008BAC40B02). The authors would like to express thanks to the anonymous reviewers for their many useful suggestions during the development of this manuscript.

REFERENCES

Albrecht, B., 1989: Aerosols, cloud microphysics, and fractional cloudiness. *Science*, **245**, 1227–1230.

Briegleb, B. P., 1992: Delta-Eddington approximation for solar radiation in the NCAR Community Climate Model. *J. Geophys. Res.*, **97**, 7603–7612.

Coakley, J. A. Jr., R. L. Bernstein, and P. A. Durkee, 1987: Effect of ship-track effluents on cloud reflectivity. *Science*, **237**, 1020–1022.

Collins, W. D., P. J. Rasch, B. E. Eaton, B. Khattaov, J. F. Lamarque, and C. S. Zender, 2001: Simulating aerosols using a chemical transport model with assimilation of satellite aerosol retrievals: Methodology for INDOEX. *J. Geophys. Res.*, **106**, 7313–7336.

Collins, W. D., P. J. Rasch, B. E. Eaton, D. W. Fillmore, J. T. Kiehl, T. C. Beck, and C. S. Zender, 2002: Simulation of aerosol distributions and radiative forcing for INDOEX: Regional climate impacts. *J. Geophys. Res.*, **107**, doi: 10.1029/2001JD001365.

Eagan, R., P. V. Hobbs, and L. Radke, 1974: Measurements of CCN and cloud droplet size distributions in the vicinity of forest fires. *J. Appl. Meteor.*, **13**, 537–553.

Forster, P., and Coauthors, 2007: Changes in Atmospheric Constituents and in Radiative Forcing. *Climate Change 2007: The Physical Science Basis. Contribution of Working Group I to the Fourth Assessment Report of the Intergovernmental Panel on Climate Change*, Solomon et al., Eds., Cambridge University Press, 131–217.

Ghan, S., R. Easter, J. Hudson, and F. M. Breon, 2001: Evaluation of aerosol indirect radiative forcing in MIRAGE. *J. Geophys. Res.*, **106**(D6), 5317–5334.

Hack, J. J., 1994: Parameterization of moist convection in the NCAR Community Climate Model, CCM2. *J. Geophys. Res.*, **99**(D3), 5551–5568.

Hack, J. J., B. A. Boville, B. P. Briegleb, J. T. Kiehl, P. J. Rasch, and D. L. Williamson, 1993: Description of the NCAR Community Climate Model (CCM2). Technical Report NCAR/TN-382+STR, National Center for Atmospheric Research, 120pp.

Han, Q., W. Rossow, and A. Lacis, 1994: Near-global survey of effective droplet radii in liquid water clouds using ISCCP data. *J. Climate*, **7**(4), 465–497.

Han, Q., W. Rossow, J. Chou, and R. M. Welch, 1998: Global variations of column droplet concentration in low-level clouds. *Geophys. Res. Lett.*, **25**, 1419–1422.

Harrison, E. F., P. Minnis, B. R. Barkstrom, V. Ramanathan, R. D. Cess, and G. G. Gibson, 1990: Seasonal variation of cloud radiative forcing derived from the earth radiation budget experiment. *J. Geophys. Res.*, **95**, 18687–18703.

Jiang, H., G. Feingold, and W. R. Cotton, 2002: Simulations of aerosol-cloud-dynamical feedbacks resulting from of entrainment of aerosols into the marine boundary layer during the Atlantic Stratocumulus Transition Experiment. *J. Geophys. Res.*, **107**(24), 4813, doi: 10.1029/2001JD001502.

Jones, A., D. L. Roberts, and M. J. Woodage, 2001: Indirect sulphate aerosol forcing in a climate model with an interactive sulphur cycle. *J. Geophys. Res.*, **106**(17), 20293–20310.

Junge, C. E., 1975: The possible influence of aerosols on the general circulation and climate and possible approaches for modelling. Appendix 10, *The Physical Basis of Climate and Climate Modelling*, GARP Publications, Series No. 16, WMO, Geneva.

Kawamoto, K., T. Nakajima, and T. Y. Nakajima, 2001: A global determination of cloud microphysics with AVHRR remote sensing. *J. Climate*, **14**, 2054–2068.

Khairoutdinov, M., and Y. Kogan, 2000: A new cloud physics parameterization in a large-eddy simulation model of marine stratocumulus. *Mon. Wea. Rev.*, **128**, 229–243.

Kiehl, J. T., J. J. Hack, G. B. Bonan, B. B. Boville, D. L. Williamson, and P. J. Rasch, 1998: The National Center for Atmospheric Research Community Climate Model: CCM3. *J. Climate*, **11**, 1131–1149.

Kristjansson, J. E., 2002: Studies of the aerosol indirect effect from sulfate and black carbon aerosols. *J. Geophys. Res.*, **107**(D15), 4246, doi: 10.1029/2001JD000887.

Kristjansson, J. E., T. Iversen, A. Kirkevag, Ø. Seland, and J. Debernard, 2005: Response of the climate system to aerosol direct and indirect forcing: Role of cloud feedbacks. *J. Geophys. Res.*, **110**, D24206, doi: 10.1029/2005JD006299.

Lohmann, U., and J. Feichter, 1997: Impact of sulfate aerosols on albedo and lifetime of clouds: A sensitivity study with the ECHAM4 GCM. *J. Geophys. Res.*, **102**, 13685–13700.

Lohmann, U., J. Feichter, C. Chuang, and J. E. Penner, 1999: Prediction of the number of cloud droplets in the ECHAM GCM. *J. Geophys. Res.*, **104**(D8), 9169–9198.

Lohmann, U., and J. Feichter, 2005: Global indirect aerosol effects: A review. *Atmospheric Chemistry and Physics Discussions*, **5**, 715–737.

Lohmann, U., K. Broekhuizen, R. Leaitch, N. Shantz, and J. Abbatt, 2004: How efficient is cloud droplet formation of organic aerosols? *Geophys. Res. Lett.*, **31**, L05108, doi: 10.1029/2003GL018999.

Martin, G., D. Johnson, and A. Spice, 1994: The measurement and parameterization of effective radius of droplets in warm stratocumulus clouds. *J. Atmos. Sci.*, **51**, 1823–1842.

Menon, S., A. D. D. Genio, D. Koch, and G. Tselioudis, 2002: GCM Simulations of the Aerosol Indirect Effect: Sensitivity to Cloud Parameterization and Aerosol Burden. *Journal of Aerosol Science*, **59**, 692–713.

Ming, Y., V. Ramaswamy, P. A. Ginoux, L. W. Horowitz, and L. M. Russell, 2005: Geophysical Fluid Dynamics Laboratory general circulation model investigation of the indirect radiative effects of anthropogenic sulfate aerosol. *J. Geophys. Res.*, **110**, D22206, doi: 10.1029/2005JD006161.

Nakajima, T., A. Higurashi, K. Kawamoto, and J. E. Penner, 2001: A possible correlation between satellite-derived cloud and aerosol microphysical parameters. *Geophys. Res. Lett.*, **28**(7), 1171–1174.

Pincus, R., and M. B. Baker, 1994: Effect of precipitation on the albedo susceptibility of clouds in the marine boundary layer. *Nature,* **372**, 250–252.

Ramaswamy, V., and Coauthors, 2001: Radiative forcing of climate change. *Climate Change 2001: The Scientific Basis. Contribution of Working Group I to the Third Assessment Report of the Intergovernmental Panel on Climate Change*, Houghton et al., Eds., Cambridge University Press, 349–416.

Rasch, P. J., and J. E. Kristjansson, 1998: A comparison of the CCM3 model climate using diagnosed and predicted condensate parameterizations. *J. Climate*, **11**, 1587–1614.

Reid, J. S., T. F. Eck, S. A. Christopher, P. V. Hobbs, and B. Holben, 1999: Use of the Angstrom exponent to estimate the variability of optical and physical properties of aging smoke particles in Brazil. *J. Geophys. Res.*, **104**(D22), 27473–27490.

Rotstayn, L. D., 1999: Indirect forcing by anthropogenic aerosols: A global climate model calculation of the effective-radius and cloud-lifetime effects. *J. Geophys. Res.*, **l04**, 9369–9380.

Slingo, A., 1989: A GCM parameterization for the shortwave radiative properties of clouds. *J. Atmos. Sci.*, **46**, 1419–1427.

Slingo, J. M., 1987: The development and verification of a cloud prediction scheme for the ECMWF model. *Quart. J. Roy. Meteor. Soc.*, **113**, 899–927.

Sundqvist, H., 1978: A parameterization scheme for nonconvective condensation including prediction of cloud water content. *Quart. J. Roy. Meteor. Soc.*, **104**, 677–690.

Takemura, T., T. Nozawa, S. Emori, T. Y. Nakajima, and T. Nakajima, 2005: Simulation of climate response to aerosol direct and indirect effects with aerosol transport-radiation model. *J. Geophys. Res.*, **110**, D02202, doi: 10.1029/2004JD005029.

Twomey, S. A., 1977: The influence of pollution on the shortwave albedo of clouds. *J. Atmos. Sci.*, **34**, 1149–1152.

Warner, J., and S. A. Twomey, 1967: The production and cloud nuclei by cane fires and the effect on cloud droplet concentration. *J. Atmos. Sci.*, **24**, 704–706.

Wu, T., and G. Wu, 2004: An empirical formula to compute snow cover fraction in GCMs. *Adv. Atmos. Sci.*, **21**, 529–535.

Wu, T. W., and Coauthors, 2008: The Beijing Climate Center atmospheric general circulation model: Description and its performance for the present-day. *Climate Dyn.*, doi: 10.1007/s00382-008-0487-2.

Xie, P., and P. A. Arkin, 1997: Global precipitation: A 17-year monthly analysis based on gauge observations, satellite estimates, and numerical model outputs. *Bull. Amer. Meteor. Soc.*, **78**, 2539–2558.

Yan, H., 1987: Design of a nested fine-mesh model over

the complex topograph, Part two: Parameterization of the subgrid physical processes. *Plateau Meteorology*, **6** (Suppl.), 64–139. (in Chinese)

Zhang, G. J., and M. Mu, 2005: Effects of modifications to the Zhang-McFarlane convection parameterization on the simulation of the tropical precipitation in the National Center for Atmospheric Research Community Climate Model, version 3. *J. Geophys. Res.*, doi: 10.1029/2004JD005617.

Zhang, H., Z. L. Wang, P. W. Guo, and Z. Z. Wang, 2009: A modeling study of the effects of direct radiative forcing due to carbonaceous aerosol on the climate in East Asia. *Adv. Atmos. Sci.*, **26**(1), 57–66.

Zhang, M., W. Lin, C. S. Bretherton, J. J. Hack, and P. J. Rasch, 2003: A modified formulation of fractional stratiform condensation rate in the NCAR community atmospheric model CAM2. *J. Geophys. Res.*, **108**(D1), 4035, doi: 10.1029/2002JD002523.

Zhao, C. S., D. Y. Peng, and Y. Duan, 2005: The impacts of sea-salt and nss-sulfate aerosols on cloud microproperties. *Chinese Journal of Applied Meteorological Science*, **16**(4), 417–425. (in Chinese)